PHYSICAL REVIEW B 85, 245122 (2012)

Thermally assisted tunneling transport in La_{0.7}Ca_{0.3}MnO₃/SrTiO₃: Nb Schottky-like heterojunctions

F. A. Cuellar, ^{1,2} G. Sanchez-Santolino, ^{1,2} M. Varela, ^{1,2,3} M. Clement, ^{2,4} E. Iborra, ^{2,4} Z. Sefrioui, ^{1,2} J. Santamaria, ^{1,2} and C. Leon ^{1,2}

¹GFMC, Departamento de Física Aplicada III, Facultad de Física, Universidad Complutense de Madrid, Campus Moncloa, 28040 Madrid, Spain

²CEI Campus Moncloa, UCM-UPM, 28040 Madrid, Spain

³Materials Science & Technology Division, Oak Ridge National Laboratory, Oak Ridge, Tennessee 37831, USA ⁴GMME-CEMDATIC, Escuela Técnica Superior de Ingenieros de Telecomunicaciones. Universidad Politécnica de Madrid, Campus Moncloa. 28040 Madrid, Spain

(Received 9 April 2012; published 20 June 2012)

We report on the electrical transport properties of all-oxide $La_{0.7}Ca_{0.3}MnO_3/SrTiO_3$:Nb heterojunctions with lateral size of just a few micrometers. The use of lithography techniques to pattern manganite pillars ensures perpendicular transport and allows exploration of the microscopic conduction mechanism through the interface. From the analysis of the current-voltage characteristics in the temperature range 20–280 K we find a Schottky-like behavior that can be described by a mechanism of thermally assisted tunneling if a temperature-dependent value of the dielectric permittivity of $SrTiO_3$:Nb (NSTO) is considered. We determine the Schottky energy barrier at the interface, $qV_B=1.10\pm0.02$ eV, which is found to be temperature independent, and a value of $\xi=17\pm2$ meV for the energy of the Fermi level in NSTO with respect to the bottom of its conduction band.

DOI: 10.1103/PhysRevB.85.245122 PACS number(s): 73.30.+y, 73.40.-c

I. INTRODUCTION

Interfaces in complex oxide heterojunctions provide an interesting playground to investigate novel electronic phases driven by the strong influence of symmetry breaking on electron correlations. Remarkable examples are the formation of a two-dimensional electron gas at the interface between two insulators in LaAlO₃/SrTiO₃, and the induced magnetism in Ti atoms in LaMnO₃/SrTiO₃ heterostructures.³ Understanding the induced electronic states at complex oxide interfaces not only is interesting from a fundamental viewpoint but also has considerable technological potential.⁴ Novel device functionalities might be designed by taking advantage of the exotic ground states nucleating at these interfaces, which could be eventually modified by controlling the charge density. Interface band profiles in several complex oxide heterojunctions have been previously investigated by optical spectroscopy⁵ and transport measurements⁶ in order to gain a basic knowledge of the electronic reconstruction at the interface between complex oxides and the differences from interfaces in conventional semiconductor heterojunctions. In particular, the manganite-titanate interface has been the focus of considerable research interest, 7-14 and very recently the engineering of the interface dipole has allowed the design of a perovskite oxide-based transistor.¹⁵

Here we report on the fabrication and electrical transport characterization of La Ca manganite doped titanate heterojunctions La_{0.7}Ca_{0.3}MnO₃/SrTiO₃:Nb, with lateral size of just a few micrometers. The smaller bandwidth of La_{0.7}Ca_{0.3}MnO₃ (LCMO) (compared to La_{0.7}Sr_{0.3}MnO₃ (LSMO)) makes the electronic ground state in this material more susceptible to small changes of the charge density or other correlation parameters, which may give rise to interesting functionalities. In SrTiO₃:Nb (NSTO) electrons are doped from shallow levels into the otherwise empty 3*d* conduction band. The discontinuity in the work function at the interface drives electrons from

the titanate into the e_g conduction band of the manganite¹⁶ until the induced electric dipole produces a flat profile of the chemical potential. We have used lithography techniques to pattern pillars which ensure perpendicular transport with well-defined current geometry. This allows the details of the microscopic conduction mechanism in our junctions to be explored. From the analysis of the current-voltage curves as a function of temperature, we determine the Schottky-like behavior of these heterojunctions and the importance of thermally assisted tunneling in their transport properties, even close to room temperature. We also estimate the Schottky energy barrier at the interface, which is found to be temperature independent from room temperature down to 20 K. We discuss also the importance of a temperature-dependent value of the relative permittivity of NSTO for an appropriate description of the experimental data.

II. EXPERIMENT

A stoichiometric La_{0.7}Ca_{0.3}MnO₃ target was used to grow epitaxial thin films (40-60 nm thick) onto (001) SrTiO₃ single crystal $10 \times 5 \times 1 \text{ mm}^3$ substrates doped with 0.02 at. %Nb, by using a high oxygen pressure (3.4 mbar) and a hightemperature (900 °C) rf sputtering system. 17-19 Such a growth technique allows us to obtain single-phase high-crystallinequality films, as confirmed by scanning transmission electron microscopy (STEM), x-ray diffraction (XRD), and x-ray reflectometry measurements. High-angle annular dark-field (HAADF) images of the interface between the substrate and the manganite layer were obtained using a Nion Ultra STEM microscope operated at 100 keV. Figure 1 shows that LCMO layers grow epitaxially, (001) oriented, and are flat over long lateral distances. Micrometer-sized (60–160 μ m²) junctions (square and rectangular shapes) were defined by using conventional optical lithography and Ar plasma etching

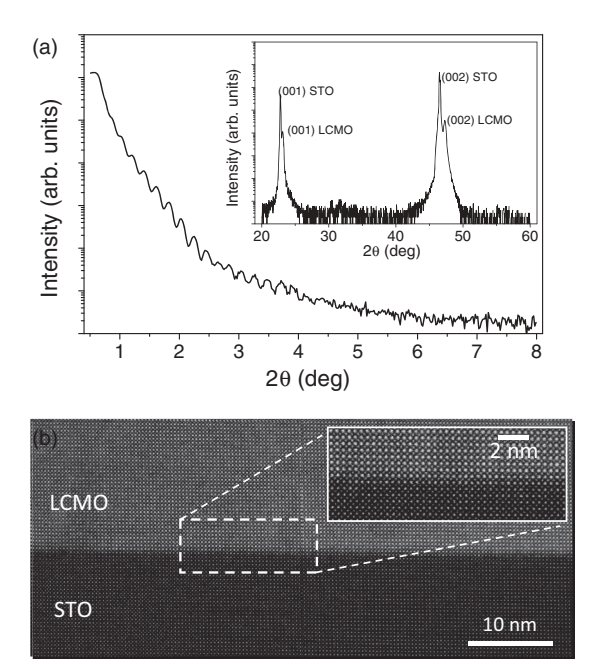


FIG. 1. (a) X-ray reflectivity and diffraction (inset) patterns of a 40-nm-thick LCMO layer. The presence of a large number of finite-thickness oscillations in the reflectivity data indicates that the samples are flat over long lateral distances. High-angle XRD evidences the epitaxial growth of the manganite layer with the (001) orientation on the STO substrate. (b) Low- and high- (inset) magnification HAADF images of the interface between the substrate and the manganite layer. The dashed box marks the region of the high-magnification image.

after sputtering a 90-nm-thick amorphous-Au layer to be used as electrical contact to the LCMO layer. The whole system is covered with an amorphous 300-nm-thick SiO₂ layer for electrical passivation of exposed surfaces. A reactive ion etching system was used to define holes in the SiO₂ layer to allow sputtering of metal electrodes (10 nm Ti/200 nm Mo) on top of the Au layer. The Ti layer is then in direct contact with the Au layer above LCMO in each junction, and in direct contact with the NSTO substrate at the electrode pads [see inset to Fig. 2(a)]. Ti is used instead of Au to contact NSTO in order to avoid undesirable Schottky (NSTO-Au) rectifying contacts.²⁰ Finally, the Mo pads were contacted by using ultrasound wire bonding. Thus the fabricated heterostructures consist of Schottky junctions (where LCMO is the metal and NSTO is the semiconductor) with Au and Ti contacts, respectively. Electrical measurements were performed in a closed-circuit helium cryostat from room temperature down to 20 K. A Keithley 2400 source measure unit was used to measure *I-V* characteristics. From a total of 42 junctions fabricated, six showed a Schottky-like behavior, while others were either open or shunted and could not be measured. This is typical statistics when measuring perpendicular transport in our micrometersized pillars fabricated by an optical litography process.

III. RESULTS AND DISCUSSION

Figure 2(a) shows current density-voltage (J-V) characteristics at different temperatures between 20 and 280 K, evidencing the good rectifying behavior of LCMO-NSTO junctions in the whole temperature range as demonstrated

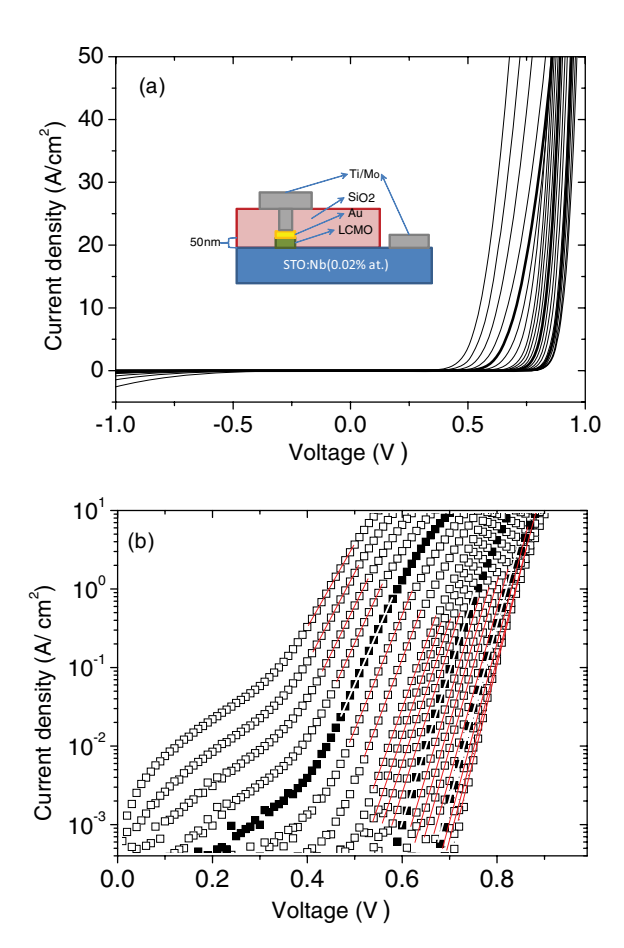


FIG. 2. (Color online) (a) Current density–voltage characteristics of a $7 \times 14 \ \mu m^2$ LCMO/NSTO heterojunction, with a 60-nm-thick LCMO layer, at several temperatures (280, 260, 240, 220, 200, 180, 160, 140, 130, 120, 110, 100, 90, 80, 70, 60, 50, 40, 30, and 20 K from the left to the right). Isotherms at 200, 100, and 50 K are plotted as thicker lines for clarity. Inset is a schematic layout of the fabricated junctions showing the electrodes used (see text). (b) Semilogarithmic plot of the current density–voltage characteristics in the forward-bias region at several temperatures (280, 260, 240, 220, 200, 180, 160, 140, 130, 120, 110, 100, 90, 80, 70, 60, 50, 40, 30, and 20 K from the left to the right). Data at 200, 100, and 50 K are plotted as solid symbols for clarity. Solid lines are fits to Eqs. (1) and (2) in the text.

by the strong asymmetry of J - V curves in the linear scale at forward and reverse bias. Figure 2(b) shows the forward-bias region of the same J - V curves but in a semilogarithmic scale, where the exponential dependence of the current density on applied bias can be better observed, as shown by the straight lines at each isothermal curve. The presence of a distinct region at low bias is also evident for temperatures above 160 K which is characterized by a weaker exponential dependence (and thus a lower slope on the semilogarithmic scale). Although it is still an open question how to model the band alignment and transport properties in these manganite-titanate interfaces, it has been previously reported that they are well described by assuming a metal (LCMO)-n-type semiconductor (NSTO) Schottky junction, where the contribution of holes to the transport process is negligible and essentially only electrons contribute to the current.^{8,21} According to the Schottky junction model, the thermionic current at forward bias can be approximated as

$$J_F \approx J_S(T) \exp(qV/nkT)$$
 (1)

for applied bias $V \gg kT/q$, and where q is the electronic charge, k is the Boltzmann constant, T is the junction temperature, and n is the ideality factor which equals 1 for an ideal diffusion mechanism.²² The saturation current density $J_S(T)$ is given by

$$J_S(T) = A^* T^2 \exp(-q V_B / kT), \tag{2}$$

with V_B the Schottky barrier height and A^* the effective Richardson constant.²² We use $A^* = 156 \text{ A cm}^{-2} \text{ K}^{-2}$, which corresponds to an effective electron mass $m^*/m_0 = 1.3$ for NSTO, ²³ and thus we are able to obtain the values of V_B and n at each temperature by fitting experimental data for J - Vcurves to Eqs. (1) and (2) [see the solid lines in Fig. 2(b)]. It is important to remark that we have limited these fits to the intermediate-bias region to avoid considering the slight deviation from an exponential dependence due to a small series resistance effect that is observed at the highest bias and the presence of the distinct region mentioned above at low bias for the highest temperatures, which may be influenced by the recombination of carriers or a different transport process. As shown in Fig. 3(a), the ideality factor n deviates from unity at high temperature ($n \sim 1.7$) and increases strongly at low temperature, reaching unphysical values. In view of the good structural quality of the titanate/manganite interface shown by the STEM images (see Fig. 1), we can dismiss that the high values of n are due to some damage of the interface resulting from the sputtering technique used in the fabrication of the junctions. Similarly, Fig. 3(b) shows that the Schottky barrier height qV_B derived from the fits is found to decrease from about $qV_B = 0.66$ eV at room temperature to unphysically small values approaching zero at the lowest temperatures $(qV_B = 0.10 \text{ eV} \text{ at } T = 20 \text{ K})$. Figure 3(c) and its inset show that the saturation current density is not thermally activated in the whole temperature range as expected from Eq. (2), but there is a weak exponential temperature dependence at low temperatures pointing to the importance of a tunneling mechanism contributing to the current, ^{24,25} when there is not enough available thermal energy to overcome the barrier.

Similar deviations of the current-voltage characteristics from an ideal thermionic emission have been previously reported in heterojunctions of NSTO with other transitionmetal oxides, ^{7–10,26} and thermionic-field emission (thermally assisted tunneling) has been proposed as a possible mechanism that may explain the observed results.8 In particular, as described below in more detail, a thermionic-field emission process would explain the almost temperature-independent slope observed in $\log_{10} J - V$ curves at low temperatures [see Fig. 2(b)]. The presence of a thermally assisted tunneling process in these LCMO-NSTO heterojunctions is sketched in Fig. 4, illustrating that the electrons between the Fermi level E_F and the bottom of the conduction band can tunnel from the semiconductor (NSTO) to the metal (LCMO) if they are first thermally excited to a higher energy (close to E_m in the figure) below the top of the barrier. In the thermally assisted tunneling regime the forward-bias J-V characteristics can

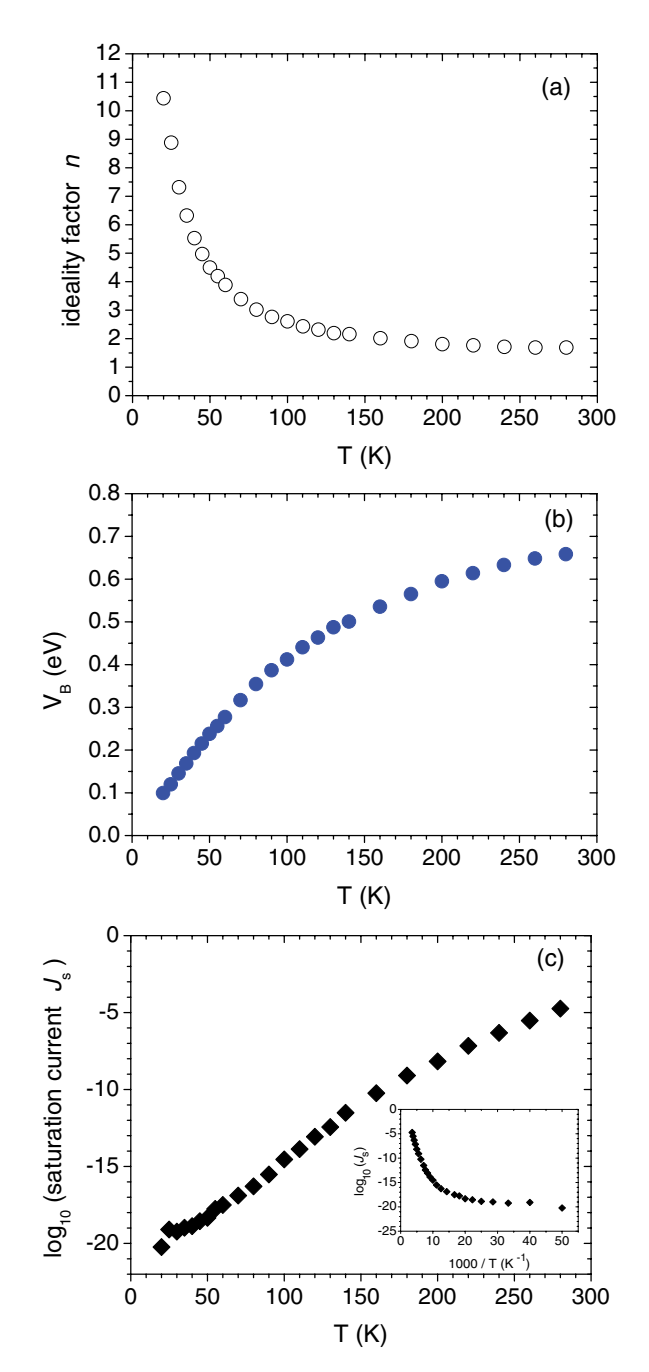


FIG. 3. (Color online) Temperature dependence of the ideality factor n (a), the Schottky barrier height V_B (b), and the saturation current density J_s (c), as obtained from the fits shown in Fig. 2(b).

be written as²⁷

$$J_F = J_S(T) \exp(qV/E_0), \tag{3}$$

with an energy E_0 that depends on temperature according to

$$E_0 = E_{00} \coth(E_{00}/kT),$$
 (4a)

$$E_{00} = \frac{qh}{4\pi} \left(\frac{N_d}{m^* \varepsilon_r \varepsilon_0} \right)^{1/2}, \tag{4b}$$

where h is the Planck constant, N_d is the donor concentration in the semiconductor ($N_d = 1.7 \times 10^{19} \, \mathrm{cm}^{-3}$ according to the nominal value of 0.02 at. % Nb doping in the NSTO substrate),

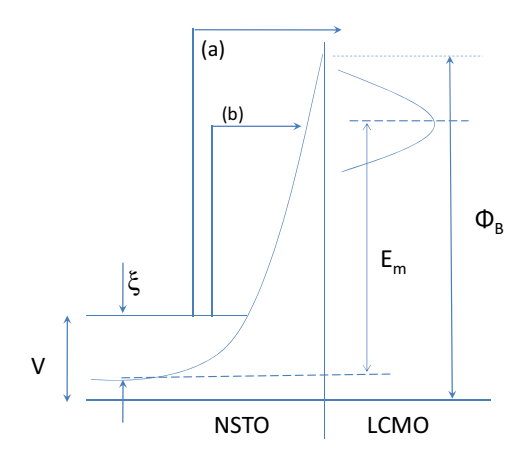


FIG. 4. (Color online) Sketch of the potential profile for a LCMO/NSTO Schottky junction under a forward bias V. The arrows represent thermoionic emission (a) and thermally assisted tunneling (b) of electrons across the junction from the semiconductor NSTO to the metallic LCMO.

 ε_r is the relative dielectric permittivity of NSTO, and ε_0 is the permittivity of vacuum. The temperature dependence of the saturation current in Eq. (3) is given by

$$J_{S}(T) = \frac{A^{*}T^{2}\pi^{1/2}E_{00}^{1/2}[q(V_{B} - V) + \xi]^{1/2}}{kT\cosh(E_{00}/kT)} \times \exp\left(\frac{\xi}{kT} - \frac{qV_{B} + \xi}{E_{0}}\right), \tag{5}$$

where ξ is the energy difference between the Fermi level E_F and the bottom of the conduction band of the semiconductor.

By comparing Eqs. (3) and (1), the values of E_0 as a function of temperature can be directly obtained from those previously calculated for n, since at any fixed temperature the slope of the $\log_{10} J - V$ curve is determined by $E_0 = nkT$. Figure 5 shows that E_0 depends weakly on temperature below 60 K, with a value $E_0 = 19 \pm 1$ meV, while it is roughly proportional to temperature close to room temperature, as is indeed expected from the asymptotic temperature dependence given by Eq. (4a). However, as also shown in Fig. 5, the E_0 values obtained at each temperature from J - V curves cannot be well described by using Eqs. (4) if the value of E_{00} given by Eq. (4b) is assumed to be temperature independent. The dashed line in the figure represents the best fit to this expression and it clearly deviates from the values determined from experimental data. This could be explained as a consequence of a temperature dependence of the permittivity ε_r of NSTO. It is well known that the bulk permittivity of SrTiO₃ is about 300 at room temperature and increases strongly toward a value of 24 000 at low temperature since SrTiO₃ is an incipient ferroelectric material.²⁸ It has also been shown previously that under a high electric field of the order of 10^7 – 10^8 V/m, like that expected in the space-charge region close to the interface with LCMO, the permittivity can be much lower, and although the temperature dependence of ε_r under such high electric fields is not well established, it has been reported that it still shows a slight increase when the temperature decreases.²⁹ Thus we have fitted E_0 in Fig. 4 at each temperature by using Eq. (4) to obtain a temperature-dependent value for the dielectric permittivity $\varepsilon_r(T)$ as a fit parameter. The values obtained for the dielectric

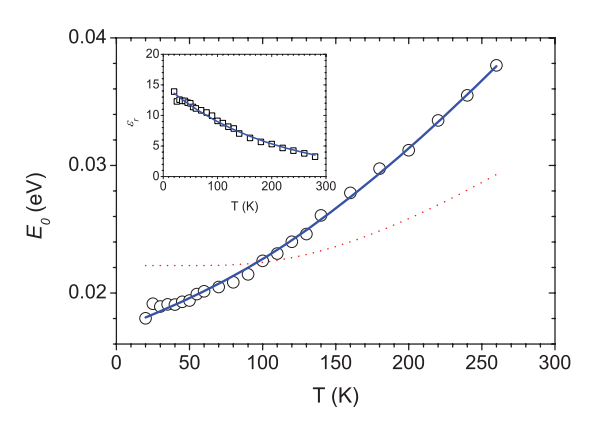


FIG. 5. (Color online) Open circles represent the energy $E_0 = nkT$ determined as the inverse of the slope in $\ln J - V$ plots (see text). The dotted line is the best fit to Eq. (4a) by using a constant value for the parameter E_{00} defined by Eq. (4b). The solid line is the best fit to Eq. (4a) by allowing a temperature dependence of E_{00} through a temperature-dependent value of the dielectric permittivity of NSTO. A weakly exponential decay of the dielectric permittivity is assumed, which is shown in the inset (solid line), to describe the temperature dependence of the values of the dielectric permittivity of NSTO (open squares) obtained from the fits to Eq. (4) of E_0 data shown in the main panel.

permittivity ε_r of NSTO in the space-charge region are shown in the inset to Fig. 4. Its temperature dependence is found to be well described by a weakly decaying exponential (solid line in the inset) and, remarkably, the values obtained for ε_r as well as their temperature dependence are reasonable according to the expected behavior under a high electric field as previously mentioned. We find $\varepsilon_r \sim 3$ at room temperature and a slight increase toward $\varepsilon_r \sim 14$ at T=20 K. These values for the dielectric permittivity might seem quite small for SrTiO₃, but are actually comparable to those previously determined in other similar heterojunctions.^{8,30} The small values could result from the high electric field existing in the space-charge region,³¹ or from the presence of a low-permittivity layer at the NSTO surface. 7,32 Interestingly, although ε_r was considered to be temperature independent in previous analyses of similar J-V characteristics, capacitance measurements indicated that ε_r has a temperature dependence similar to the one we obtain here.⁸ Note also that in order to obtain the dielectric permittivity values, we used Eq. (4), where we assumed that the donor concentration N_d is equal to the nominal value of Nb doping in the NSTO substrate. However, it is possible that N_d actually takes a larger value, in particular close to the interface with the LCMO film,³¹ which would lead us to underestimate the dielectric permittivity values. The solid line in the main panel of Fig. 5 represents the temperature dependence of E_0 given by Eqs. (4) when the phenomenological exponential temperature dependence obtained for ε_r is used. As is clearly observed from the figure, there is remarkable agreement with E_0 values determined from experimental data, supporting our hypothesis of a temperature-dependent ε_r and consequently of a temperature-dependent value of E_{00} .

Further evidence of the existence of a thermally assisted tunneling regime dominating the electrical properties of these LCMO-NSTO heterojunctions is obtained from the analysis of the saturation current and its temperature dependence.

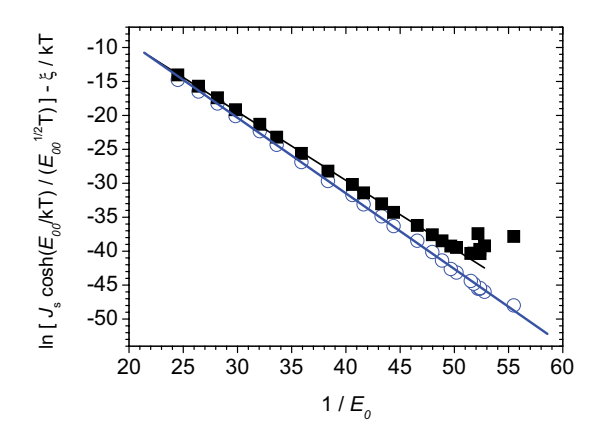


FIG. 6. (Color online) Plots of $\ln[J_S(T)\cosh(E_{00}/kT)/E_{00}^{1/2}T] - \xi/kT$ as a function of $1/E_0$ for $\xi = 0$ meV (solid squares) and for $\xi = 17$ meV (open circles). Solid lines are linear fits to the data between 280 and 60 K for the case of $\xi = 0$ meV, and to the data in the whole temperature range, between 280 and 20 K, for the case of $\xi = 17$ meV.

By simple inspection of Eq. (5) it is concluded that if the energy ξ is small compared with qV_B and also small enough compared with kT (that is, at enough high temperature), we can neglect its contribution and thus the slope of a plot of $\ln[J_S(T)\cosh(E_{00}/kT)/E_{00}^{1/2}T]$ vs $1/E_0$ gives the value of -qV directly. The solid symbols in Fig. 6 show that such a plot is indeed well described by a linear dependence for temperatures above 50 K, and a value of the Schottky barrier height $qV_B = 1.10 \pm 0.02$ eV is obtained from the slope of the corresponding linear fit. We can go a step further and try to account for the observed departure at temperatures lower than 50 K by considering the effect of a nonzero value for the energy ξ and, moreover, try to estimate its value from the experimental data. Note that in a closer inspection of Eq. (5) we can easily find that $\{\ln[J_S(T)\cosh(E_{00}/kT)/E_{00}^{1/2}T] - \xi/kT\}$ vs $1/E_0$ plots must show a linear dependence in the whole temperature range, and the slope is then given by $-(qV_B + \xi)$. Such a plot, where the existence of the ξ energy term in Eq. (5) is taken into account, is represented by open symbols in Fig. 6. The linear behavior found for this plot, down to the lowest temperature, by using $\xi = 17$ meV, is indeed remarkable, and thus from the corresponding linear fit we obtain a value of $qV_B = 1.10 \pm 0.02$ eV for the Schottky barrier height. The value determined for the Schottky barrier height is actually very close to that recently estimated, $qV_B \sim 1.25 \text{ eV}$, from measurements at room temperature of the quantum efficiency of the photocurrent induced in similar LCMO/NSTO heterojunctions.³³ It is also quite remarkable that the value $\xi = 17(\pm 2)$ meV deduced from the experimental data is in very good agreement with that estimated by assuming a Fermi distribution of the carriers, $N=(2m^*\xi/\hbar^2)^{3/2}/3\pi^2$, and complete ionization of donor impurities in NSTO, which gives $\xi=18$ meV. These findings, together with the fact that the Schottky barrier is found to be essentially temperature independent when a thermally assisted tunneling mechanism at the interface is assumed, give an additional and strong support to our interpretation that this mechanism dominates the behavior of the current-voltage characteristics in LCMO-NSTO heterojunctions.

IV. CONCLUSIONS

In summary, we have fabricated $\sim 100 - \mu \text{m}^2$ -sized LCMO-NSTO heterojunctions showing good rectifying behavior, and, from the analysis of J - V curves at forward bias, we can conclude that transport is dominated by thermally assisted tunneling across the Schottky-like barrier formed at the manganite-titanate interface. A value of $qV_B=1.10\pm$ 0.02 eV for the Schottky barrier height is obtained, independent of temperature, and in good agreement with previous estimates from photocurrent measurements in similar heterojunctions. We estimate the relative permittivity value of NSTO in the space-charge region to be about $\varepsilon_r \sim 3$ at room temperature and that slightly increases toward $\varepsilon_r \sim 14$ when the temperature decreases to T = 20 K. These values are actually small for SrTiO₃, but they are similar to those estimated in other manganite-titanate heterojunctions, and may result from the large electric field values reached in the spacecharge region close to the interface. It is quite surprising that "classical" transport models developed for junctions involving conventional semiconductors describe quite well the behavior of our heterostructures based on strongly correlated electron systems. In fact, it has been pointed out recently that simple one-electron band schemes also seem to describe well the band profile of these junctions as probed by light and transport experiments.⁵ Future work will be necessary to clarify the role of the electron correlations in the transport mechanisms of oxide junctions.

ACKNOWLEDGMENTS

This work has been supported by the Spanish MICINN under Projects No. MAT2008-06517, No. MAT2010-18933, No. MAT2011-27470, and No. CSD2009-00013 (IMAGINE), by CAM under PHAMA Grant No. S2009/MAT-1756, and by an ERC Starting Investigator Award, Grant No. 239739 STEMOX (G.S.S.). Research at ORNL (M.V.) was sponsored by the Materials Sciences and Engineering Division of the US Department of Energy.

¹H. Y. Hwang, Y. Iwasa, M. Kawasaki, B. Keimer, N. Nagaosa, and Y. Tokura, Nat. Mater. **11**, 103 (2012).

²A. Ohtomo and H. Y. Hwang, Nature (London) **427**, 423 (2004).

³J. Garcia-Barriocanal, J. C. Cezar, F. Y. Bruno, P. Thakur, N. B. Brookes, C. Utfeld, A. Rivera-Calzada, S. R. Giblin, J. W. Taylor,

J. A. Duffy, S. B. Dugdale, T. Nakamura, K. Kodama, C. Leon, S. Okamoto, and J. Santamaria, Nat. Commun. 1, 82 (2010).

⁴J. Chakalian, A. J. Millis, and J. Rondinelli, Nat. Mater. **11**, 92 (2012).

- ⁵M. Nakamura, A. Sawa, J. Fujioka, M. Kawasaki, and Y. Tokura, Phys. Rev. B **82**, 201101(R) (2010).
- ⁶A. Sawa, A. Yamamoto, H. Yamada, T. Fujii, M. Kawasaki, J. Matsuno, and Y. Tokura, Appl. Phys. Lett. **90**, 252102 (2007).
- ⁷F. M. Postma, R. Ramaneti, T. Banerjee, H. Gokcan, E. Haq, D. H. A. Blank, R. Jansen, J. C. Lodder, and J. Lodder, J. Appl. Phys. **95**, 7324 (2004).
- ⁸T. Susaki, N. Nakagawa, and H. Y. Hwang, Phys. Rev. B **75**, 104409 (2007).
- ⁹A. Ruotolo, C. Y. Lam, W. F. Cheng, K. H. Wong, and C. W. Leung, Phys. Rev. B **76**, 075122 (2007).
- ¹⁰Y. W. Xie, J. R. Sun, D. J. Wang, S. Liang, W. M. Lu, and B. G. Shen, Appl. Phys. Lett. **90**, 192903 (2007).
- ¹¹W. M. Lu, J. R. Sun, D. J. Wang, Y. W. Xie, S. Liang, Y. Z. Chen, and B. G. Shen, Appl. Phys. Lett. **92**, 062503 (2008).
- ¹²Y. Hikita, M. Nishikawa, T. Yajima, and H. Y. Hwang, Phys. Rev. B **79**, 073101 (2009).
- ¹³M. Minohara, Y. Furukawa, R. Yasuhara, H. Kumigashira, and M. Oshima, Appl. Phys. Lett. **94**, 242106 (2009).
- ¹⁴T. Y. Chien, J. Liu, J. Chakalian, N. P. Guisinger, and J. W. Freeland, Phys. Rev. B **82**, 041101 (2010).
- ¹⁵T. Yajima, Y. Hikita, and H. Y. Hwang, Nat. Mater. **10**, 198 (2011).
- ¹⁶S. Yunoki, A. Moreo, E. Dagotto, S. Okamoto, S. S. Kancharla, and A. Fujimori, Phys. Rev. B **76**, 064532 (2007).
- ¹⁷T. Endo, A. Hoffmann, J. Santamaria, and I. K. Schuller, Phys. Rev. B **54**, R3750 (1996).
- ¹⁸Z. Sefrioui, D. Arias, M. Varela, J. E. Villegas, M. A. López de la Torre, C. León, G. D. Loos, and J. Santamaría, Phys. Rev. B 60, 15423 (1999).

- ¹⁹A. Rivera, J. Santamaria, and C. Leon, Appl. Phys. Lett. **78**, 610 (2001).
- ²⁰T. Shimizu, N. Gotoh, N. Shinozaki, and H. Okushi, Appl. Surf. Sci. 117–118, 400 (1997).
- ²¹A. G. Milnes and D. L. Feucht, *Heterojunctions and Metal-Semiconductor Junctions* (Academic, New York, 1972).
- ²²S. M. Sze, *Physics of Semiconductor Devices*, 2nd ed. (Wiley, New York, 1981).
- ²³Z. Sroubek, Phys. Rev. B **2**, 3170 (1970).
- ²⁴A. R. Riben and D. L. Feucht, Solid State Electron. **9**, 1055 (1966).
- ²⁵A. Bindal, R. Wachnik, and W. Ma, J. Appl. Phys. **68**, 6259 (1990).
- ²⁶F. Y. Bruno, J. Garcia-Barriocanal, M. Torija, A. Rivera, Z. Sefrioui, C. Leighton, C. Leon, and J. Santamaria, Appl. Phys. Lett. **92**, 082106 (2008).
- ²⁷F. A. Padovani and R. Stratton, Solid State Electron. **9**, 695 (1966).
- ²⁸A. Spinelli, M. A. Torija, C. Liu, C. Jan, and C. Leighton, Phys. Rev. B **81**, 155110 (2010).
- ²⁹R. A. van der Berg, P. W. M. Blom, J. F. M. Cillesen, and R. M. Wolf, Appl. Phys. Lett. **66**, 697 (1995).
- ³⁰S. Suzuki, T. Yamamoto, H. Suzuki, K. Kawaguchi, K. Takahashi, and Y. Yoshisato, J. Appl. Phys. 81, 6830 (1997).
- ³¹O. Copie, V. Garcia, C. Bödefeld, C. Carrétéro, M. Bibes, G. Herranz, E. Jacquet, J.-L. Maurice, B. Vinter, S. Fusil *et al.*, Phys. Rev. Lett. **102**, 216804 (2009).
- ³²T. Shimizu and H. Okushi, J. Appl. Phys. **85**, 7244 (1999).
- ³³X. Y. Lu, J. R. Sun, A. D. Wei, W. W. Gao, D. S. Shang, J. Wang, Z. H. Wang, and B. G. Shen, Appl. Phys. Lett. **97**, 022502 (2010).